Int. J. Heat Mass Transfer. Vol. 28, No. 3, pp. 531–539, 1985
Printed in Great Britain

0017–9310/85 $3.00 + 0.00

Rotation-induced heat transfer in a radial flow passage in a rotating shaft

E. M. SPARROW and L. M. HOSSFELD
Department of Mechanical Engineering, University of Minnesota, Minneapolis, Minnesota 55455, U.S.A.

(*Received* 25 *May* 1984 *and in revised form* 3 *August* 1984)

Abstract—Experiments have been performed to determine the heat transfer characteristics for rotation-induced flow in a radial passage in a shaft rotating about its own axis. The experiments encompassed passages whose ends were either flush with the surface of the shaft or protruded beyond the surface. For the latter, the passage was either centered in the shaft or else was offset such that the respective ends protruded different distances from the shaft surface. In the main body of experiments, both ends of the passage were open. Supplementary experiments with only one open end and others with an internal blockage were carried out to gain insight into the pattern of fluid flow. When the passage was centered in the shaft, there was negligible fluid throughflow, but even a small offset gave rise to a significant throughflow. For the centered case, the heat transfer coefficient was insensitive to whether the passage did or did not protrude beyond the shaft. Offsetting of the passage provided significant heat transfer enhancement relative to the centered case, and even a slight offset doubled the heat transfer coefficient.

INTRODUCTION

THIS PAPER is concerned with the heat transfer characteristics of a circular passage running radially through a shaft which rotates about its own axis. Any fluid motions which occur within the passage are induced solely by the rotation. The presence of such passages affords direct contact between the interior of the shaft and the ambient fluid and may, thereby, enhance the heat transfer between the shaft and the fluid.

The passage may have various configurations, as illustrated in Fig. 1. The simplest configuration is that of Fig. 1(a), where a hole passes directly through the shaft. A more general approach is to insert a hollow tube in the hole such that the ends of the tube extend beyond the surface of the shaft. By varying the length of the inserted tube, its heat transfer surface area can be varied. Indeed, heat transfer would occur both from the bore of the tube and from that portion of the tube's outside surface which is exposed to the fluid environment. The tube may be centered in the shaft (Fig. 1(b)) or may be offset (Fig. 1(c)). Offsetting creates an imbalance of the centrifugal forces which, in turn, sets up a net flow through the tube, giving rise to enhanced heat transfer. Mechanical imbalances caused by the offsetting can be neutralized by the use of oppositely offset tubes positioned in neighboring holes.

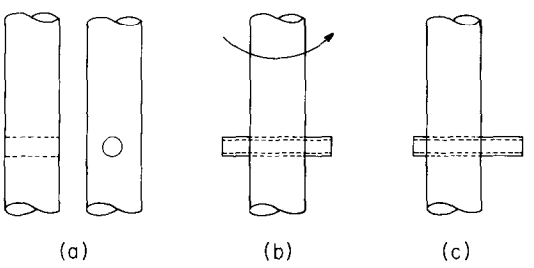

FIG. 1. Radial passages in a shaft rotating about its own axis.

Despite the potential practical importance of the just-described radial passages in shaft–fluid heat transfer, it appears that neither fundamental nor applied studies of their transfer characteristics have been reported in the literature. In the present investigation, experiments have been performed to determine these characteristics. The experiments encompassed a variety of passage configurations. These included all three configurations pictured in Fig. 1 and, for the configuration of Fig. 1(c), several offset positions were employed. For each configuration, the rotational Reynolds number was varied by almost an order of magnitude. To obtain a better understanding of the participating transfer processes, supplementary experiments were performed in which one end of the passage was sealed, thereby preventing fluid throughflow. Other experiments were carried out with a barrier positioned midway between the ends of the passage, the presence of the barrier serving to limit the size of the eddy that is situated within the passage.

Average Nusselt numbers were obtained for each of the aforementioned cases and are presented as a function of the Reynolds number. Whenever possible, generalizations were achieved via correlations involving both the Reynolds number and the geometrical parameters. The Nusselt numbers for the open-ended passages were compared with those for forced convection transitional and turbulent flow in a circular tube. Comparisons were also made between the results for the open-ended passages and those for the passages closed at one end.

As noted earlier, the physical situation investigated here has not been dealt with previously. For completeness, mention may be made of published

NOMENCLATURE

D	diameter of flow passage
D_o	outside diameter of test element tube
D_s	diameter of shaft
$\mathscr{D}$	mass diffusion coefficient
f	friction factor
K	mass transfer coefficient
L	length of flow passage
$\dot{m}$	mass transfer per unit time and area
Nu	Nusselt number
Pr	Prandtl number
R_{max}	radial distance to far end of passage
R_{min}	radial distance to near end of passage
R_{open}	radial distance to open end of passage
ΔR	offset, $(R_{max}-R_{min})$
Sc	Schmidt number
Sh	Sherwood number, $KD/\mathscr{D}$
Re	rotational Reynolds number, $\rho\omega D^2/\mu$
Re	pipe-flow Reynolds number, equations (5) and (6).

Greek symbols

μ	viscosity
ν	kinematic viscosity
ρ	density
ρ_{nw}	naphthalene vapor density at passage wall
$\rho_{n\infty}$	naphthalene vapor density in ambient
ω	angular velocity of shaft.

experiments for the case where fluid is pumped through a tube rotating about an axis perpendicular to its own axis [1]. In that case, the rate of flow passing through the tube is an independent, controlled variable. On the other hand, in the present situation, the extent of the throughflow is a dependent, uncontrolled variable.

THE EXPERIMENTS

For reasons of feasibility, flexibility, and accuracy, the naphthalene sublimation technique was used instead of direct heat transfer experiments. In general, the naphthalene technique affords smaller extraneous losses, higher measurement accuracy, and simpler fabrication and assembly than does the corresponding heat transfer experiment. Furthermore, it enables a standard boundary condition (analogous to uniform wall temperature) to be readily attained. Specific advantages for the present problem include ease of variation of the geometrical parameters and avoidance of the difficulties of conveying electric power and multiple thermocouple emfs across a rotating interface.

The mass transfer results can be transformed to heat transfer results using the well-established analogy between the two processes.

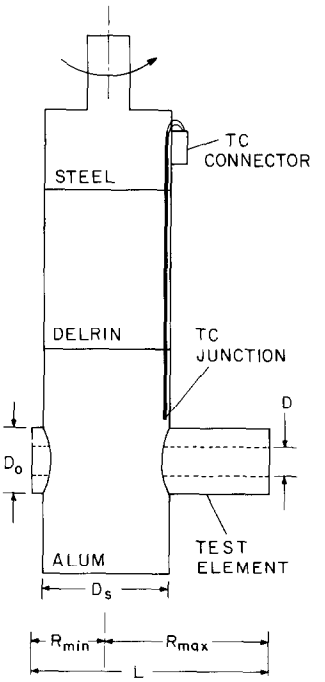

FIG. 2. Experimental apparatus.

Experimental apparatus

A schematic diagram of the experimental apparatus is presented in Fig. 2. The main components of the apparatus are a rotating shaft and a cylindrical test element which is situated in a hole in the shaft. As seen in the figure, the axis of the test element is perpendicular to that of the shaft. At its upper end, the shaft was reduced in diameter to facilitate its mating with a collet implanted in the spindle of a vertical milling machine. The milling machine served as the source of rotation. It was operated over the range from 265 to 2240 rpm in as many as nine discrete steps. Periodic measurements of the rotational speeds by both optical and electromechanical tachometers verified their constancy.

As can be seen in Fig. 2, the rotating shaft was made up of three sections, each of a different material. These sections were mated via tongue-in-groove type fits and held together with recessed screws, with the recesses filled with body putty. To ensure trueness and continuity, the assembly was machined to the final diameter D_s as a unit.

The upper portion of the shaft mated with the milling machine and was made of steel for strength. Delrin, a plastic, was used for the middle section in order to thermally isolate the test element from the frictional heating (actually, rather minimal) in the spindle of the milling machine. The lower portion of the shaft housed

the test element. It was made of aluminum because its high thermal conductivity aided in the attainment of temperature uniformity. This uniformity enhanced the accuracy of the temperature measurements and also gave rise to uniformity in the boundary condition for mass transfer (to be elaborated later).

The test element was fabricated from aluminum rod stock. Its external surface (diameter D_o) was finished to achieve a snug fit with the transverse hole in the aluminum section of the shaft. The rod was bored along its axis to provide a circular flow passage. The bore hole was further recessed, and the hollowed out space served as a mold cavity into which a layer of naphthalene was cast. As a result, the flow passage was bounded by a naphthalene surface, with its diameter being denoted by D. The flat faces at each end of the test element were of aluminum (i.e., part of the original rod). Therefore, the investigated mass transfer occurred only from the bore of the passage. Further details of the geometry of the test element will be illustrated when the casting procedure is described.

Two lengths L of the test element were employed during the course of the research. The first of these lengths corresponds to $L/D \simeq 8$ (actually, 7.99). Furthermore, for this length, $L/D_s = 1.85$, so that the ends of the test element extended beyond the surface of the shaft. Experiments were performed with the element in a centered position (Fig. 1(b)) and in various offset positions (Fig. 1(c)), the most extreme of which is that shown in Fig. 2. The extent of the offset may be characterized in terms of the quantities R_{max} and R_{min} illustrated in Fig. 2, such that the offset is given by $\Delta R = (R_{max} - R_{min})$.

Subsequent to the data runs for $L/D = 8$, the test element was reduced in length so that $L = D_s$, which yielded $L/D = 4.33$. For this length, experiments were run with the test element in the centered position ($\Delta R = 0$). This test setup was meant to simulate the situation pictured in Fig. 1(a) (i.e., a radial hole passing through the shaft), with slight deviations due to the flat end faces of the test element.

As noted in the introduction, the primary data runs—those in which both ends of the flow passage are open—were supplemented by runs in which one end of the passage was sealed. For the latter, the seal was accomplished by the use of pressure-sensitive tape. In still another set of runs, a blockage was positioned midway between the ends of the passage. The blockage was a Delrin plug machined so that it could be pressed into the bore of the passage to the desired location.

During the data runs, the test element was locked in place by set screws which were seated in grooves machined into the outside surface of the element. Appropriately positioned grooves were provided for the various investigated offsets, but in no case were the grooves exposed. The grooves and the provision of space for the mold cavity were the key factors in setting the diameter ratio D_o/D of the test element.

The key dimensions of the apparatus are $D = 1.425$ cm and $D_s = 6.17$ cm, along with the dimension ratios $D_o/D = 2.25$, $L/D = 8$ (longer passage), and $L/D = 4.33$ (shorter passage). Figure 2 is drawn to scale, so that all the less critical dimensions can be read from it in terms of those just stated.

Mass transfer surface

The procedure used for casting the naphthalene surface at the bore of the flow passage will be described with the aid of Fig. 3, which shows the setup of the mold. The mold consists of two parts. Of these, the outer part is the aluminum test element tube, while the centerbody is a highly polished aluminum shaft. The annular space between these parts is the mold cavity, into which molten naphthalene is poured during the casting procedure. The figure shows the assembled mold with the naphthalene layer in place.

The first step in the casting procedure is to remove the naphthalene remaining in the test element tube from the preceding data run. This is accomplished by melting and evaporation. Next, the centerbody is inserted into the tube as shown in Fig. 3. Then, molten naphthalene is poured into the mold cavity through a circular aperture in the side wall of the tube, and the air displaced by the naphthalene is allowed to escape through a pair of small vent holes, one adjacent to each end of the tube. When the naphthalene has solidified, the centerbody shaft is pressed out of the tube, leaving an exposed naphthalene surface whose finish is comparable to that of the polished shaft.

Unwanted bits of naphthalene that may have solidified on the outer surface of the tube during the pouring process were carefully removed and the pouring aperture and vent holes sealed with pressure-sensitive tape. The two ends of the flow passage were also sealed with tape and maintained so until the initiation of the data run.

Figure 3 displays the geometry of the inner surface of the test section tube. The hollowed-out mold cavity is seen to extend virtually along the full length of the tube. At each end of the tube, the hollow space is closed by a beveled retaining wall which terminates in a short flat lip (~ 1 mm long) against which the centerbody bears during the casting process.

Instrumentation and experimental procedure

The quantities measured for each data run include the mass of the test element (both before and after the run), the temperature of the mass transfer surface, the

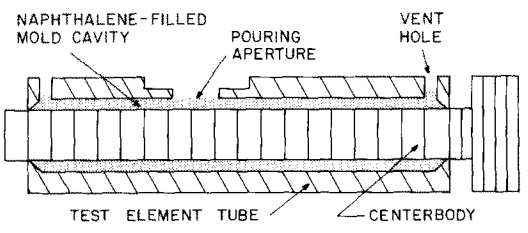

FIG. 3. Setup for casting the naphthalene surface.

ambient pressure, and the duration of the run. In addition, each run was also characterized by the rotational speed of the shaft and the geometry of the test element.

The mass of the test element was measured by a Sartorius electronic, ultraprecision, analytical balance with a resolving power of 10^{-5} g and a capacity of 166 g. Typically, the change of mass during a run was in the 0.05–0.1 g range.

For the temperature measurements, it was assumed that the temperature of the test element was identical to that of the aluminum portion of the rotating shaft adjacent to the element. Accordingly, a thermocouple junction (30-gage chromel-constantan) was embedded in a shallow depression in the aluminum surface at a distance of about 0.635 cm from the test element, as illustrated in Fig. 2. The thermocouple lead wires were laid in a shallow groove which extended from the junction to the steel section of the rotating shaft. Copper oxide cement and body putty were used to fill the groove, after which the surface was sanded smooth. As can be seen in the figure, the thermocouple leads which emerged from the upper end of the groove were attached to the socket portion of a sub-miniature, quick-connect connector taped to the side of the shaft.

Temperature measurements were not made when the shaft was actually rotating. To facilitate the temperature measurement, the rotating spindle of the milling machine was braked to an abrupt halt, and the plug portion of the thermocouple connector was mated with the socket portion. These operations were performed and the thermocouple emf read from the display of a digital voltmeter, usually within ten seconds.

The rotational speed of the shaft was set by means of the speed control buttons of the milling machine. As previously mentioned, each setting was carefully calibrated with tachometers and checked periodically for constancy.

To initiate a data run, the test element was weighed. Immediately after the weighing, both ends of the flow passage were sealed with pressure-sensitive tape to suppress measurable sublimation. Next, the test element was inserted into the shaft, which had already been set up in the milling machine, and locked in the preselected configuration (centered or offset).

Rotation was then initiated, thereby initiating a period of thermal equilibration. During this period, the ends of the flow passage were kept sealed to prevent sublimation, while the shaft was rotated at the rpm designated for the data run. Also, during this period, the temperature was read periodically, and this was continued until the temperature became steady. At this point, the tape was removed from either one or both ends of the passage, depending on the desired operating condition, and the data run proper was begun.

The duration of the run was selected to limit the average sublimation-related change in diameter of the flow passage to less than 0.0025 cm. At the end of the run, the rotation was abruptly halted, the temperature measured, and the end(s) of the flow passage sealed. Then, the test element was reweighed.

The experiments were performed in a large laboratory (~ 300 m^3), so that possible accumulations of naphthalene vapor were negligible. Entrance to the laboratory was restricted both during the equilibration period and the data run proper. As an added precaution, the windows were covered with sheets of polystyrene insulation. These measures provided a stable environment conducive to the attainment of reproducible, scatter-free data.

Data reduction

The measured change of mass during a data run, divided by the duration of the run and by the naphthalene surface area which bounded the flow passage, yields the average mass flux $\dot{m}$. With $\dot{m}$, the average mass transfer coefficient K and Sherwood number Sh follow as

$$K = \dot{m}/(\rho_{nw} - \rho_{n\infty}), \quad Sh = KD/\mathscr{D}. \tag{1}$$

In defining K, the driving potential for mass transfer was taken to be the difference between the densities of the naphthalene vapor at the wall of the flow passage and in the ambient outside the passage. Owing to the high conductivity of the surrounding aluminum and to the absence of heat sources and sinks,* the naphthalene which bounds the flow passage is isothermal. Correspondingly, the naphthalene vapor pressure at the surface-fluid interface is uniform along the flow passage. The Sogin vapor pressure–temperature relation [2] was used to evaluate the vapor pressure with the measured average surface temperature as input. In turn, using the vapor pressure and temperature as inputs, ρ_{nw} was evaluated from the perfect gas law. For the operating conditions of the experiments, $\rho_{n\infty} = 0$.

The mass diffusion coefficient $\mathscr{D}$ which appears in the Sherwood number was eliminated by means of the Schmidt number $Sc = \nu/\mathscr{D}$, with the result that $Sh = (KD/\nu)Sc$. The value of the Schmidt number is 2.5 for naphthalene diffusion in air [2].

It is to be expected that the angular velocity ω of the shaft will play a key role in establishing the value of the Sherwood number. Dimensional arguments suggest that ω should be embedded in a Reynolds-number-like dimensionless group. There are numerous candidates for the characteristic length that appears in the definition of the Reynolds number (i.e. D, L, R_{max}, R_{min}, ΔR, and even D_s). Ideally, the optimal choice of a characteristic length for the Reynolds number leads to a correlation which is insensitive to one or more of the other dimensionless groups (e.g. dimension ratios).

Exploratory correlation efforts did not reveal any such simplifications. Therefore, it was decided to use the passage diameter D as the characteristic length since it

* The latent heat requirements of the sublimation process were evaluated and shown to be negligible.

was common to all cases, thereby allowing the variations in the Reynolds number solely to reflect changes in the rotational speed. Thus,

$$Re = \rho\omega D^2/\mu. \quad (2)$$

In addition to the Reynolds number, the results will be parameterized by various dimension ratios.

RESULTS AND DISCUSSION

Passages open at both ends

The presentation will begin with the results for the passage open at both ends, and Fig. 4 has been prepared for this purpose. Attention is first focused on the upper part of the figure, where Sherwood number data are plotted as a function of the rotational Reynolds number $\rho\omega D^2/\mu$ for both of the investigated passage lengths $L/D = 4.33$ and 8. For the longer passage, the data encompass the centered case $\Delta R/D = 0$ as well as four different offsets $\Delta R/D$ ranging from 0.36 to 3.09. The length of the shorter passage is exactly equal to the diameter of the shaft, so that the passage was employed only in the centered mode.

Inspection of the figure reveals remarkable findings both with respect to the effect of offset for the longer passage and with respect to the effect of passage length for the centered mode. Relative to the centered mode, offsetting serves to increase the Sherwood number, but it is the enormous enhancements that occur at small offsets that are of special note. In particular, the Sherwood numbers for the $\Delta R/D = 0.36$ offset are about 2.1 times those for no offset. This enhancement is even more remarkable when it is realized that the $\Delta R/D = 0.36$ offset corresponds to a displacement of the tube by only 0.25 cm from the centered position (ΔR is twice the displacement).

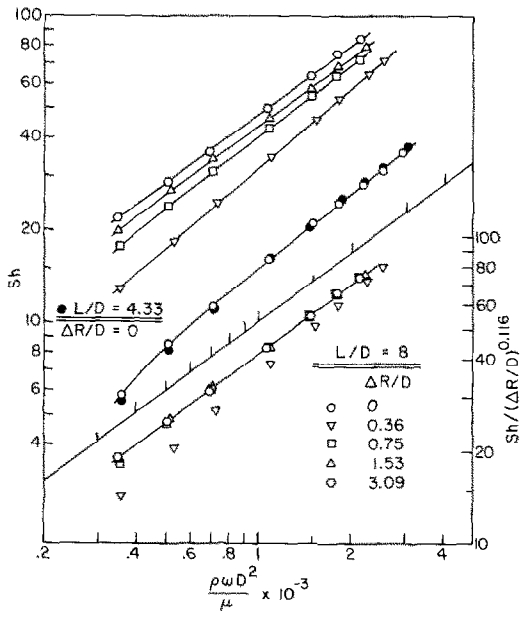

FIG. 4. Sherwood number results for passages open at both ends.

When the offset is doubled from $\Delta R/D = 0.36$ to 0.75, further significant enhancement occurs, but the increment is substantially smaller than the initial enhancement. Further doubling of the offset to $\Delta R/D = 1.53$ and then to 3.09 yields only modest gains. At the latter offset (the largest investigated here), the Sherwood numbers are 3 to 3.9 times those for no offset, depending on the Reynolds number.

The marked differences between the Sherwood numbers with and without offset are indicative of the different flow patterns which prevail in the two situations. In the presence of offset, there is a throughflow whose direction is from the R_{min} end to the R_{max} end (shorter end to longer end) of the passage, as detected by smoke. Thus, in this case, the rotation provides a pumping action.

On the other hand, for the centered case, significant throughflow is not expected. Rather, there should be a closed eddy (a pocket of recirculating fluid) extending from each end of the passage toward the interior. The eddy is driven by the drag at the passage opening which is caused by the sharp change in the tangential velocity of the fluid. Ideally, symmetry should prevail with respect to the axial midpoint of the passage such that there are identical eddies in the two halves of the passage which extend radially outward from the midpoint. In reality, it is quite likely that because the eddy motion is prone to unsteadiness, there will be asymmetries between the two halves of the passage, and throughflow may occur. However, as witnessed by Fig. 4, the throughflow, if any, should be small compared with that corresponding to a small offset.

With the effect of offsetting now established, attention is next turned to the centered orientation and to how the Sherwood number is affected by the L/D of the passage. By examining the $\Delta R/D = 0$ results for $L/D = 4.33$ and 8 in the upper diagram of Fig. 4 (filled and open circle data symbols, respectively), virtual coincidence is observed. This insensitivity of the Sherwood number to L/D is unexpected, but it can be rationalized. The greater the L/D, the larger is the drag force at the passage opening which drives the aforementioned eddy. However, since the passage length increases with L/D, the resistance to the eddy motion increases. Thus, since both the force and the resistance increase with L/D, a neutralization may occur which yields a constant Sherwood number.

The constancy of the Sherwood number implies the constancy of the mass (or heat) transfer coefficient. Since the rate of mass (or heat) transfer depends on the product of the transfer coefficient and the transfer surface area, it is apparent that the larger L/D passage is an effective means of increasing the rate of transfer. Furthermore, the larger the L/D, the greater is the *outside surface area of the tube that can participate in* the transfer process. Notwithstanding the virtues of the centered passage with larger L/D, it is still inferior to a slightly offset passage of the same L/D.

Further study of the upper graph of Fig. 4 indicates that the Sherwood number increases rapidly with the rotational Reynolds number. Aside from a slight drop at the lowest Reynolds number in some cases, the Sherwood–Reynolds data fall along straight lines with virtually no scatter. Thus, power-law relations of the form

$$Sh = C(\rho\omega D^2/\mu)^n \tag{3}$$

can be fitted to the data. The C and n values obtained via least squares are listed in Table 1. Equation (3), together with Table 1, can be used with confidence to extrapolate the data of Fig. 4 to higher Reynolds numbers.

An attempt to correlate the effect of offset on the Sherwood number results proved to be fruitful at the larger offsets because of the nearly common Reynolds number dependence that prevails (see Table 1). An excellent large-offset correlation was found to be

$$Sh = 0.234(\Delta R/D)^{0.116}(\rho\omega D^2/\mu)^{0.75}. \tag{4}$$

This equation is plotted in the lower graph of Fig. 4 in the form $Sh/(\Delta R/D)^{0.116}$ versus Reynolds number, along with the data for the $\Delta R/D = 0.36, 0.75, 1.53$, and 3.09 offsets. Examination of the figure reveals that equation (4) is a satisfactory representation of the results for $\Delta R/D \geqslant 0.75$.

As noted in the introduction, there are no results in the published literature which are directly comparable to those found here. Notwithstanding this, it is desirable to make perspective-giving comparisons. To this end, the present results will be compared with those for forced convection heat transfer in a circular tube. Among the available correlations for that case, the Gnielinski modification [3] of the well-established Petukhov–Popov equation covers the widest Reynolds number range ($Re > 2300$) because it spans both the transition and turbulent regimes. According to Gnielinski, the average Nusselt number for a tube of length L/D is given by

$$Nu = \frac{(f/8)(Re-1000)\,Pr[1+(D/L)^{2/3}]}{1+12.7(f/8)^{1/2}(Pr^{2/3}-1)} \tag{5}$$

where

$$f = [1.82\log(Re)-1.64]^{-2}. \tag{6}$$

In equations (5) and (6), Re denotes the conventional Reynolds number for forced convection pipe-flow, and it should not be confused with the rotational Reynolds number of the present experiments.

Table 1. Values of C and n for equation (3)

L/D	$\Delta R/D$	C	n
4.33	0	0.0559	0.809
8	0	0.0559	0.809
	0.36	0.0783	0.869
	0.75	0.194	0.773
	1.53	0.259	0.742
	3.09	0.271	0.748

For mass transfer, the Nusselt and Prandtl numbers appearing in equation (5) are replaced by the Sherwood and Schmidt numbers. With these changes and after setting $Sc = 2.5$ for naphthalene sublimation in air, equation (5) provides the value of Sh for given values of Re and L/D. Suppose that L/D is taken to be either 4.33 or 8 (the present L/D values). Then, equation (5) can be used to answer the following question: What is the pipe-flow Reynolds number Re which yields the same Sherwood number as was obtained at a given value of $\rho\omega D^2/\mu$ in the present experiments?

The equivalent pipe-flow Reynolds numbers are plotted in Fig. 5 as a function of $\rho\omega D^2/\mu$, where the various curves correspond to the two investigated L/D values and to the various offsets $\Delta R/D$. Note that $Re > 2300$ in accordance with the range of validity of equation (5).

In essence, Fig. 5 provides a "feel" for the $\rho\omega D^2/\mu$ parameter by relating it to a pipe-flow Reynolds number which yields the same Sherwood number. The figure shows that for the $\rho\omega D^2/\mu$ range of the present experiments, the equivalent pipe flows would, for the most part, be characterized by Reynolds numbers below 10,000. While such Reynolds numbers are moderate, they are not uncommon in heat exchanger practice. Furthermore, larger angular velocities than those employed here (i.e., >2240 rpm) would result in correspondingly larger values of the equivalent pipe Reynolds number. Thus, it may be concluded that the mass (heat) transfer coefficients which occur in a radial passage in a rotating shaft are not uncommonly low relative to those for heat exchange devices in general.

Passages open at one end

The experiments performed with passages open at only one end were undertaken to provide perspective for the results obtained for passages open at both ends. In Fig. 6, Sherwood number results for various one-end-open passages are presented. Comparisons between the one-end- and two-end-open passages will be made in later figures.

When only one end of the passage is open, a

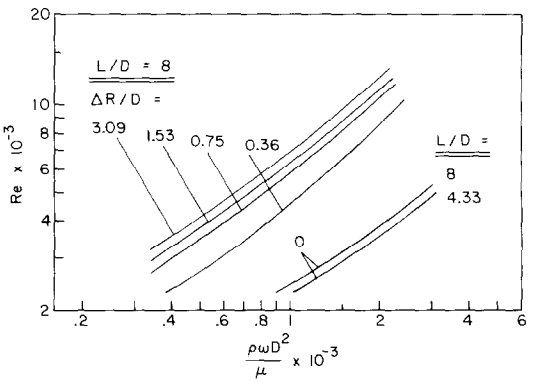

FIG. 5. Values of the pipe Reynolds number Re and $\rho\omega D^2/\mu$ which yield the same Sherwood number.

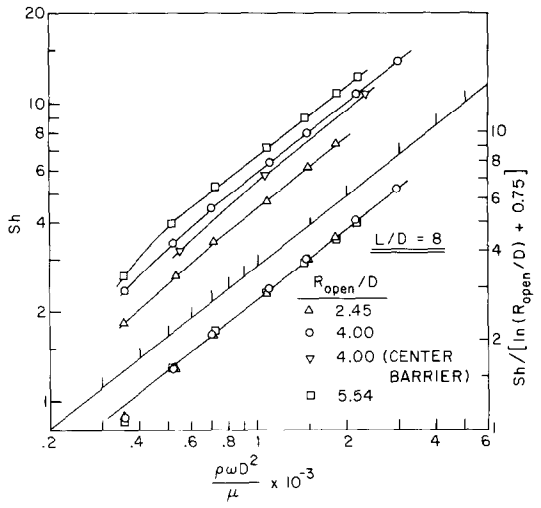

FIG. 6. Sherwood number results for passages open at one end.

throughflow is not possible. Instead, eddy motion (i.e., recirculation) within the passage is to be expected. The eddy motion is driven by the drag force at the open end. For a given angular velocity ω, the drag should depend on the radial distance R_{open} between the center of rotation and the opening. Correspondingly, the results will be parameterized by R_{open}/D.

In the upper graph of Fig. 6, the Sherwood number results are plotted as a function of the Reynolds number for $R_{open}/D = 2.45$, 4, and 5.54. For all three cases, the overall length of the passage was $L/D = 8$. An additional set of data was collected for the $R_{open}/D = 4$ case in which, as noted earlier, a Delrin plug was inserted as a barrier. The barrier prevented fluid flow across the midplane of the passage so that the eddy motion was confined between the midplane and the open end (the other end of the passage was sealed with tape).

Inspection of the data shows that the Sherwood number increases as the distance between the center of rotation and the open end of the passage increases. The higher Sherwood numbers are due to the more vigorous eddy motions which are encountered in passages of higher tip velocity (i.e., larger R_{open}). Also of interest is the fact that the Sherwood number results for the $R_{open}/D = 4$ case with the center barrier are only slightly lower than those for the same R_{open}/D but without the barrier. In the latter, the eddy motion is free to fill the entire length of the passage while for the former it is confined to half the tube length. The closeness of the respective Sherwood numbers suggests that even without the barrier, the eddy motion does not penetrate much beyond the midplane of the tube.

Further inspection of the data indicates that the Sherwood–Reynolds distributions have about the same straight-line slope for the various values of R_{open}/D. This fact facilitated the correlation

$$Sh = 0.0122[\ln(R_{open}/D) + 0.75](\rho\omega D^2/\mu)^{0.784}. \quad (7)$$

This correlation (solid line) is compared with the experimental data in the lower graph of Fig. 6. All of the data except that for the lowest Reynolds number are very well described by the correlating equation. The use of the equation as an interpolation and extrapolation formula appears warranted, except for Reynolds numbers below 500.

A comparison of Sherwood number results for one-end-open and two-end-open passages in the presence of offset is made in Fig. 7. The figure corresponds to a passage of fixed length ($L/D = 8$) situated at a fixed offset ($\Delta R/D = 3.09$) and operated in three different modes. In one mode, the short end of the tube is open ($R_{open}/D = 2.45$), while in the second mode the long end is open ($R_{open}/D = 5.54$). Both ends of the tube are open in the third mode. Data points have been omitted from Fig. 7 because they have already been shown in prior figures.

Figure 7 shows that there are enormous differences between the Sherwood numbers for the one-end-open and two-end-open passages in the presence of offset. The observed differences are, respectively, factors of seven and ten when comparing the long-end-open and short-end-open passages with the two-end-open passage. This finding reaffirms the key role played by fluid throughflow in establishing the magnitude of the Sherwood number.

Attention is now turned to comparing the one-end- and two-end-open passages operating in the centered mode. Ideally, neither of these configurations should experience a throughflow. Since eddy motions are driven from the open end of the passage, it is expected that the Sherwood numbers will be higher when there are two open ends than when there is only one open end.

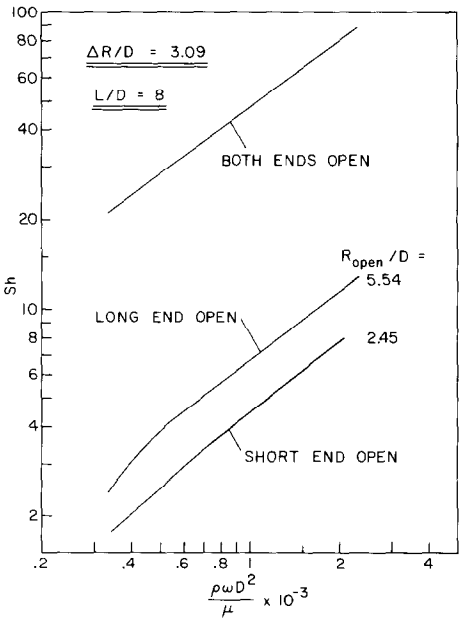

FIG. 7. Comparison of Sherwood numbers for one-end-open and two-end-open passages in the presence of offset.

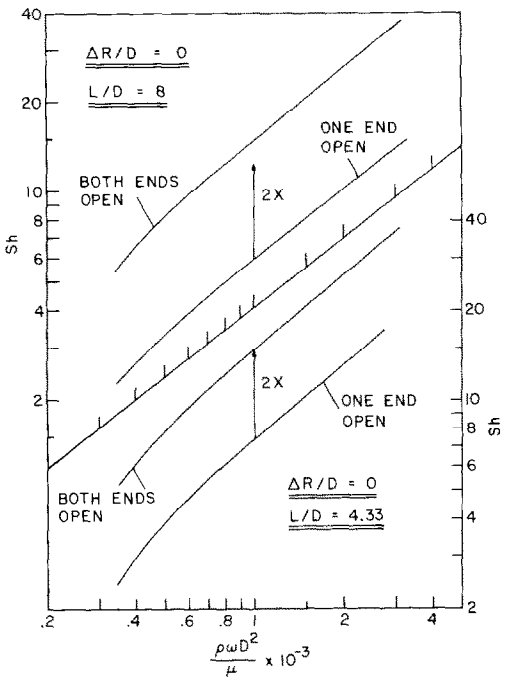

FIG. 8. Comparison of Sherwood numbers for one-end-open and two-end-open passages in the centered mode (i.e., no offset).

This expectation is fulfilled by the results presented in Fig. 8, where the lower and upper graphs respectively correspond to $L/D = 4.33$ and 8. Each graph contains curves representing the Sherwood number results for the one-end-open and two-end-open passages. Also shown is a vertical line designated as $2\times$ which depicts the doubling of the magnitude of the one-end-open curve.

The figure shows that the Sherwood numbers for the two-end-open passage are of the order of twice those of the one-end-open passage. This suggests that for the latter, the eddy motion driven from its open end penetrates about half the length of the passage. When both ends are open, there is an eddy system driven from each end, each penetrating half the passage length.

On the basis of these results, it may be concluded that for a centered passage open at both ends, there is little, if any, throughflow.

CONCLUDING REMARKS

The experiments reported here seemingly constitute the first investigation of the heat transfer characteristics for rotation-induced flow in radial passages in a shaft rotating about its own axis. A number of different passage configurations were investigated. Among these, the simplest was, in effect, a radial hole passing through the shaft. More complex configurations were attained by inserting a tube in the radial hole such that the ends of the tube extended beyond the surface of the shaft. Experiments were performed both with the tube centered in the shaft and with the tube offset such that its two ends protruded different distances beyond the shaft surface.

In the main body of experiments, both ends of the passage were open. In supplementary experiments, undertaken to gain insight into the pattern of fluid flow in the passage, one end of the passage was sealed, leaving only one end open. As a further supplement, a barrier was inserted to prevent flow across the axial midplane of the passage.

Careful examination of the results suggested that there was no significant throughflow of fluid when the passage was centered in the rotating shaft. Throughflow occurred when the passage was offset, and there is evidence that the throughflow was significant even for small offsets.

For the centered mode, the heat transfer coefficient was found to be the same regardless of whether the passage did or did not protrude beyond the surface of the shaft. Since the protruding passage has a larger heat transfer surface area than the non-protruding passage, it has a greater heat transfer capability. This capability is further supplemented by possible heat transfer from the outer surface of the protruding passage.

Even a slight offset resulted in a significant heat transfer enhancement ($\sim$ a factor of two) relative to the centered mode. Further offsetting provided additional enhancement, but in progressively smaller increments.

Possible mechanical imbalances due to offsetting can be neutralized by use of oppositely offset, neighboring passages.

REFERENCES

1. Y. Mori, T. Fukada and W. Nakayama, Convective heat transfer in a rotating radial circular pipe, *Int. J. Heat Mass Transfer* **14**, 1807–1824 (1971).
2. H. H. Sogin, Sublimation from disks to air streams flowing normal to their surfaces, *Trans. ASME* **80**, 61–71 (1958).
3. V. Gnielinski, New equations for heat and mass transfer in turbulent pipe and channel flow, *Int. Chem. Engng.* **16**, 359–368 (1976).

TRANSFERT THERMIQUE INDUIT PAR ROTATION DANS UN PASSAGE RADIAL POUR UN ARBRE TOURNANT

Résumé—Des expériences permettent de déterminer les caractéristiques du transfert thermique pour un écoulement induit par rotation dans un passage radial pour un arbre tournant autour de son axe. Les expériences concernent des passages dont les extrémités sont au ras de la surface de l'arbre ou bien dépasse cette surface. Dans ce dernier cas, le passage est soit centré dans l'arbre, soit compensé de telle sorte que les extrémités respectives dépassent à différentes distances de la surface. Dans la partie principale des expériences, les deux extrémités du passage sont ouvertes. Des expériences supplémentaires avec seulement une extrémité ouverte, et d'autres avec un blocage interne, sont faites pour mieux connaitre la configuration de l'écoulement du fluide. Quand le passage est centré dans l'arbre il y a un écoulement négligeable, mais même une faible compensation donne un écoulement sensible. Dans le premier cas, le coefficient de transfert thermique est insensible au fait que le passage soit ou non compensé du côté de l'arbre. La compensation du passage provoque un accroissement sensible du transfert thermique par rapport au cas centré, et même une légère compensation double le coefficient de transfert thermique.

DER WÄRMEÜBERGANG IN EINEM RADIALEN STRÖMUNGSKANAL EINER ROTIERENDEN WELLE

Zusammenfassung—Zur Bestimmung des Wärmeübertragungs-Verhaltens einer durch Drehung induzierten Strömung in einem radialen Strömungskanal einer sich um die eigene Achse drehenden Welle wurden Versuche durchgeführt. Die Versuche erstreckten sich über Strömungskanäle, deren Enden mit der Wellenoberfläche abschlossen oder über die Wellenoberfläche hinausragten. Im letzten Fall war der Strömungskanal zum einen in der Welle zentriert, zum anderen so versetzt, daß die Enden unterschiedlich weit über die Wellenoberfläche hinausragten. In der überwiegenden Zahl der Experimente waren beide Enden des Kanals offen. Zusätzliche Versuche mit nur einem offenen Ende oder mit einem internen Verschluß wurden durchgeführt, um einen Einblick in die Strömungsform zu erhalten. War der Kanal in der Welle zentriert, so konnte nur eine geringe Durchströmung festgestellt werden. Eine kleine Verschiebung des Kanals brachte eine merkliche Durchströmung. Für den Fall des zentrierten Kanals war der Wärmeübergang unabhängig davon, ob der Kanal über die Wellenoberfläche hinausragte oder nicht. Eine Verschiebung des Kanals erzeugte eine merkliche Erhöhung des Wärmeübergangs im Vergleich zum zentrierten Kanal. Schon eine kleine Verschiebung verdoppelte den Wärmeübergangskoeffizienten.

ТЕПЛООБМЕН В КАНАЛЕ, РАДИАЛЬНО ЗАКРЕПЛЕННОМ НА СТЕРЖНЕ, ВРАЩАЮЩЕМСЯ ВОКРУГ СОБСТВЕННОЙ ОСИ

Аннотация—Проведены эксперименты по определению характеристик теплообмена в канале, закрепленном радиально на стержне, вращающемся вокруг собственной оси, что обуславливало поток газа в канале. Эксперименты проводились с каналами, концы которых находились либо заподлицо с поверхностью стержня, либо были выдвинуты. Во втором случае канал был либо симметричен относительно оси стержня, либо смещен таким образом, что соответствующие концы отодвинуты на разные расстояния от поверхности стержня. В большинстве экспериментов оба конца канала были открыты. Чтобы понять структуру течения жидкости был проведен ряд дополнительных опытов только с одним открытым концом и серия экспериментов, когда конец канал был закрыт изнутри. В случае осесимметричного расположения канала относительно стержня наблюдалось пренебрежимо малое сквозное течение жидкости, но даже небольшая несимметрия приводит к возникновению существенного потока. В осесимметричном случае коэффициент теплообмена не изменялся в зависимости от того, были ли концы канала выдвинуты относительно поверхности стержня, или нет. Смещение канала увеличивало теплообмен по сравнению со случаем осесимметричного расположения и даже небольшая несимметрия удваивала коэффициент теплообмена.